Accelerated electric curing of steel-fibre reinforced concrete

Domenico Cecini [a,*], Simon A. Austin [b], Sergio Cavalaro [b], Alessandro Palmeri [b]

[a] Loughborough University, Centre for Innovative Construction Engineering (CICE), Epinal Way, Loughborough LE11 3TU, UK
[b] Loughborough University, School of Architecture, Building & Civil Engineering, Epinal Way, Loughborough LE11 3TU, UK

HIGHLIGHTS

- Similar effectiveness to steam curing in accelerating strength development.
- Slightly detrimental effect on the composite mechanical behaviour performance.
- A more porous microstructure at the fibre-matrix interface.

ARTICLE INFO

ABSTRACT

This paper evaluates the effect of electric curing on the mechanical properties and microstructure of steel fibre reinforced concrete. Specimens subjected to electric curing, steam curing and without curing were tested for compressive and residual flexural tensile strengths at different ages. The fibre-matrix contact area after pull-out was characterized by means of scanning electron microscopy. Although electric cured specimens had consistently smaller residual flexural strengths than steam cured specimens, differences were not statistically significant. Results derived from this study confirm the feasibility of applying electric curing for the production of elements made with steel-fibre reinforced concrete.

1. Introduction

Curing conditions play a crucial role in the hydration of the binder and in achieving the performance expected from the hardened material [1]. In the precast industry, curing is often synonymous with the application of heat to shorten demoulding times and to increase productivity. One can appreciate the importance of accelerated curing to the manufacturer's rate of production by considering that to reach the demoulding strength in some cases requires more than a day (several days for prestressed concrete) as opposed to hours when accelerating curing is adopted, and thus the economic viability of precast plants significantly relies on accelerated curing [2].

Steam Curing (SC) is the most common method used in precast plants to achieve high temperature cycles while ensuring abundant moisture supply [2]. Although reliable and relatively easy to control, SC has poor energy efficiency and generates temperature gradients inside the elements, thus inducing internal stresses. In other words, SC suffers the limitations of being a surface-heating method, therefore it is physically limited by thermal conductivity of the medium and maximum permissible temperature. Moreover, its on-site deployment is unfeasible in most cases due to the large equipment required (steam generators, ducts and conveyors, etcetera).

Electric methods are relatively unexplored alternatives, which generate heat by means of the Joule effect [3,4]. Indirect or direct methods can be distinguished. For the indirect method, surface or embedded electric resistors (or the reinforcement bars) are deployed to supply heat; however, regardless of the actual positioning of the heating elements, indirect electric curing remains a surface-heating method, with the physical limitations mentioned above. Conversely, for the direct method electricity is run through the concrete, either by applying a voltage to the reinforcement bars (i.e. using them as electrodes) or by means of purposely embedded electrodes [3]. The direct Electric Curing method (EC) has received relatively little attention with regard to research and it is the focus of this study.

* Corresponding author.
  E-mail addresses: D.Cecini@Lboro.ac.uk (D. Cecini), S.A.Austin@Lboro.ac.uk (S.A. Austin), S.Cavalaro@Lboro.ac.uk (S. Cavalaro), A.Palmeri@Lboro.ac.uk (A. Palmeri).

EC is a volume-heating method, with virtually no limitation to the power density that can be provided, in this being similar to microwave heating [5]. As heat is not transferred through the mould, it can be insulated and EC can achieve high energy efficiency. Also, EC requires relatively compact machinery with no moving parts, hence it is reliable, simple to maintain and compatible with on-site applications [4]. On the downside, the implementation of EC requires significant electrical power and specific engineering know-how about how fresh concrete conducts electricity.

The largest market of Steel Fibre Reinforced Concrete (SFRC) is in industrial flooring and ground bearing slabs thanks to its enhanced crack control and local redistribution capacity [6]. Structural applications where the fibre reinforcement completely replaces conventional bars have also appeared in recent years. The prime example is found in precast tunnel lining segments [7,8] along with other precast elements. Significantly, the enhanced bulk electrical conductivity of SFRC allows lower working voltages and/or higher power densities, favouring the use of EC.

Despite that, to the authors' best knowledge, only one published paper [9] (in French) has addressed the application of EC to SFRC. Although no detrimental effect of EC was observed on compressive and flexural (cracking) strengths, the study did not evaluate the influence of EC on the post-cracking residual strength provided by the combined mechanical action of the fibres and the matrix. This might well be a critical aspect, as the higher conductivity of the metal could induce differential temperature and electrochemical phenomena around the fibres, thus affecting the microstructural characteristics and post-cracking mechanical performance of the composite which are essential for the design of elements in service and ultimate limit states. Inevitably, the lack of scientific knowledge and of solid experimental evidence remains to date a barrier to the use of EC in practice.

The aim of this paper is to evaluate the effects of direct EC on the mechanical properties and microstructural characteristics of SFRC in comparison with SC and Normal (unaided) Curing (NC). An extensive experimental campaign was undertaken envisaging realistic application scenarios. In total, 108 prismatic specimens measuring 150x150x550 mm³ were cast and subjected to curing regimes with either EC, SC or NC. An EC rig, specially designed and built for this study, allowed matching of the temperature evolution attained inside the concrete specimen during SC in a climatic chamber, which enables a fair comparison between the two accelerated curing methods (SC and EC).

Thermal and electrical data were collected throughout the curing process. After that, the flexural behaviour of the beams was assessed according to [10], paying special attention to the residual tensile response. Then, cubes were sawn from the beams and characterized through the inductive method to assess the content and orientation of fibres [11–13], in order to determine the influence of variations in fibre distribution between specimens in the comparisons. The cube specimens were later used in compressive tests [14] and Barcelona indirect tension tests (the latter test is described in [15] and adapted according to [16–18]). Finally, Scanning Electron Microscopy (SEM) was undertaken along with Energy-Dispersive X-ray spectroscopy (EDX) to investigate the microstructure at the fibre-matrix interface.

This study improved our understanding of the consequences of EC on concrete elements, with and without steel fibres. It also serves as a reference for future scientific research; the results presented in this paper may prompt further exploration of the potential for practical applications of EC in SFRC elements. An example can be found in novel applications of self-compacting concrete proposed by Reymann [19] and Cecini et al. [20] for precast and cast-in-situ, respectively.

2. Literature review

Direct EC (Electric Curing) has been used on a commercial scale in Russia since 1933, both in precast plants and for in-situ casting, although no reported use for elements made with SFRC was found. A wide body of literature addressing EC from the former Soviet Union is reported by Krylov [21], along with his own research undertaken at the NIIZhB (Research Institute of Concrete and Reinforced Concrete). In comparison, studies and applications in the Western world have been scarcer and limited to precast elements, perhaps due to the generally warmer climate.

Bredenkamp [22] investigated the effect of EC on Portland cement-based concrete in comparison to NC, measuring the compressive strength evolution from 4 h to 28 days, with the goal of optimising curing strategies. Constant intensities of electric field ranging from 300 to 500 V/m were examined. EC was finished either after a given exposure time or upon reaching a total input energy of 76 kWh/m³. However, in neither case was the control based on the temperature. Despite reaching about 50% of 28-day strength in just 4 h, the strength of specimens subjected to EC was lower compared to that of specimens subjected to NC after 80 h. Even though the magnitude of the detrimental effect in terms of the strength difference after 28 days was not reported, it was deemed acceptable.

Wilson [23] performed tests using a variable transformer and real-time adjustment of the input power by temperature-controlled closed-loop. This work provided a detailed report of the electrical parameters involved in EC. The initial resistivity of fresh concrete was about 8 Ωm and, thanks to insulation applied to the specimens, a total energy input of less than 40 kWh/m³ was sufficient to complete the temperature cycle. Nevertheless, only 24-h compressive strengths were reported, ignoring any subsequent strength evolution. Heritage [24] also conducted testing of temperature-controlled EC with target temperatures of 60 and 80 °C achieved through a linear rise of 40 °C/h, after a 3 h delay before heating. No reduction of the 28-day compressive strength compared to NC was observed at 60 °C, while about 10% lower values were reported when the target temperature was 80 °C.

Kafry [4] addressed the industrial aspects of deploying EC with case studies on precast tunnel segments and in-situ casting of a multi-storey building, pointing out potential productivity gains for on-site construction. More recently, Wadhwa [25] also reported the potential use of EC both on- and off-site and provided data from an experimental campaign. In addition to assessing the compressive strength of cubes, the authors tested half-scale reinforced slabs and checked compliance with the relevant local code.

None of the previous studies performed a back-to-back comparison of EC and SC under approximately equivalent conditions, nor did they consider the possibility of applying EC on SFRC. The only exception is the paper of Paillere and Serano [9] in French, who applied EC to $100 \times 100 \times 400$ mm³ beams containing 0.0, 0.5, 1.0 or 1.5 vol% of steel fibres. These fibres were straight, had a length of 30 mm and an aspect ratio (length-to-diameter) of 75. Normal or lightweight aggregates were used to produce the concrete that was tested at ages in the period of 1–90 days after casting for flexural cracking and compressive strengths (however, post-cracking residual strengths were not assessed). Also, several slabs up to $100 \times 1200 \times 1600$ mm³ were cast to compare heating effectiveness, collect resistivity data and measure required voltages.

EC showed better homogeneity of the temperature field inside the specimen than SC, but the rate of temperature rise was faster near the electrodes. At a fibre volume of 1%, an eight-fold reduction of resistance in comparison with Plain Concrete (PC) was reported, and the strength of the electric field required for curing ranged

between 31 and 87 V/m. According to the authors, lower working voltages (or higher power densities at equal voltage) could be applied thanks to the resistivity reduction realised by the steel fibres. Moreover, they envisage the exploitation of Ohmic heating beyond curing, i.e. for the heating of hardened concrete members once put into service.

It is widely accepted [21,26,27] that the liquid phase (i.e. the pore solution at later stages) is the current-conductive component of Portland cement-based concrete. The amount and composition of the liquid phase change substantially from concrete mixing to setting and hardening. The maximum value of conductivity is observed 2–4 h after mixing. Then, a rapid decrease of conductivity takes place as water is bound by hydrating cement particles, thus reducing the amount of free liquid phase [27,28]. The conductivity of the pore solution is also affected by the temperature, which modifies the concentration of electrolytes and the mobility of ions. Even though a direct influence of an electric field on the hydration kinetics cannot be completely ruled out, Krylov [21] indicates that neither beneficial nor detrimental effects on the structure and properties of PC were ever reported. The predominant effect was linked to the temperature variation caused by the electric current.

According to Krylov [21], transitional resistance appears at the electrode interface due to a double electric layer formed by electrons in the metal and ions in the liquid phase. This creates an obstacle to the passage of electric current from the metal to concrete and may cause electrochemical phenomena, such as expansion of air bubbles and drying caused by migration and evaporation of moisture near the electrodes. This aspect is highly relevant when applying EC to SFRC as each metal fibre embedded in the concrete matrix effectively acts as an electrode, bridging across two areas at different electric potential. This could potentially affect the microstructural properties of the fibre-matrix interfacial transition zone and the post-cracking response of SFRC.

3. Experimental programme

The selection of materials and design of experiments aimed at simulating realistic application scenarios, as explained below.

3.1. Materials and mix composition

A high-performance concrete that remains highly flowable after the incorporation of steel fibres was prepared with the mixture composition shown in Table 1. A significant proportion of fines was included to obtain highly fluid concrete, typical for precasting to guarantee smooth surface finishing [29]. Mixes with 0, 35 and 70 kg/m^3 of steel fibres (equivalent to 0%, 0.45% and 0.9% by volume) in substitution of the equivalent volume of sand were proposed, following the mix definition described by Ferrara [30]. The fibres had double-hooked ends, a length of 60 mm, an aspect ratio of 65, tensile strength of 2300 MPa; 3183 steel fibres have the weight of one kg [31]. The nomenclature used to refer to the mixes include the letter f and the fibre content by weight per cubic meter, as in f00, f35 and f70.

3.2. Mixing and casting

Mixing was performed in batches of 50 L by means of a drum mixer. The fibres, total water amount minus one litre, gravel, sand, fly ash and silica fume were mixed for 10 min. Then, cement and the remaining litre of water were added, and mixing

was continued for 20 more minutes. The time 0 for the assessment of the age of the concrete was taken as the moment in which the cement was introduced. The water temperature was adjusted to 22 °C (±1 °C) at the moment of casting. The whole batch was discharged in a hopper which was then positioned on the edge of a mould with 4 beam sectors placed over a vibrating table to cast sets of 4 prismatic specimens, as shown in Fig. 1.

Each mould held 4 digital thermistors that were embedded in the concrete to measure the temperature field inside the specimen. These sensors were longitudinally positioned 55 and 210 mm apart from each end of the mould (see Figs. 1 and 2). Although thermocouples would have provided a more punctual information on the sectional gradients, they could not be used as their measurement capacity was affected by the electric current.

In the case of specimens subjected to EC, flat 150 × 150 mm^2 and 1 mm thick stainless-steel electrodes were positioned at the far opposite ends of the moulds, so that concrete could be cast against them and consistently create the same interface. The electrodes were stiffened by 10 mm-thick Perspex plates glued on the back; a central bolt protruded 25 mm into the concrete was connected to prevent relative movement during casting and handling (see Fig. 2).

The complete casting of the 4 specimens typically took about 20 s. Low intensity vibration was performed by activating the vibrating table at medium power for a duration dependent on the flowability of the mix (10 s for f00, 2 times 10 s with one-minute interval for f35, and 3 times 10 s with one-minute intervals for f70). The whole production procedure was defined and strictly repeated to reduce the inherent uncertainty of manual scooping and its effects on fibre orientation [32]. The moulds were covered with a polythene film after casting to limit the loss of moisture. A later check of cut sections showed consistent and satisfactory compaction and no sign of segregation.

3.3. Curing

The waiting period between mixing of cement and starting of temperature cycle was 5.5 h. This time was necessary not only to allow demoulding operations and setting up the specimens in the curing rig; this delay has also been shown to be critical to avoid detrimental effects from thermal expansion during heat accelerated curing [33].

From 5.5 to 24.0 h, processing of specimens was specific to the curing method. From 24 h to 7 days, specimens (except those tested at 1 day) were submerged in water. This procedure was considered necessary to neutralise any possible effect due to different moisture supply during the initial 24 h [34]. After that, specimens remained in air indoor conditions.

Fig. 1. Detail of casting of specimens.

Table 1
Mixture compositions.

Component	Type	Content (kg/m^3)			Ratio to cement
		f00	f35	f70	
Cement	CEM-I 52.5R	400			
Silica fume	"grade 940U"	40			0.10
Fly ash	EN450-1 Fineness Cat. S; LOI Cat. B	200			0.50
Sand	0–2 mm	838	832	826	
Gravel	4–10 mm	670			
Water		170			0.425
Superplasticizer	Mapei NRG1012	6.4			0.016
Fibre	Dramix 5D®	0	35	70	
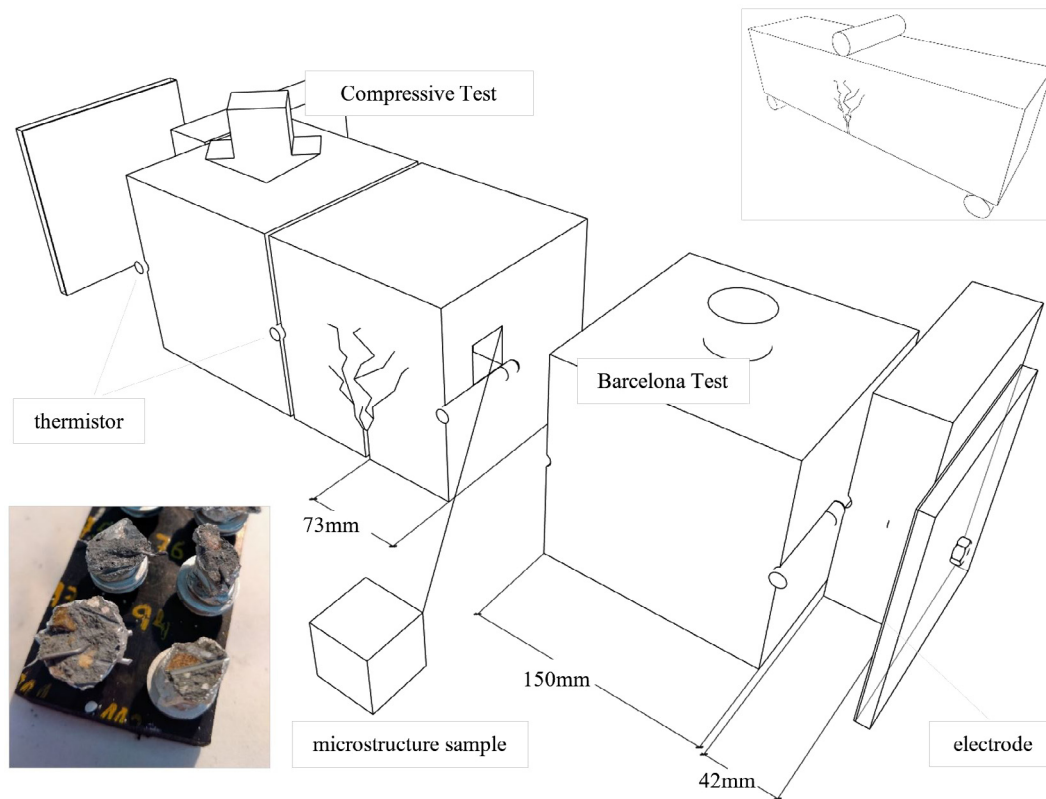
Fig. 2. Detail of a bending specimen being subsequently cut into cubes for compression and double punch Barcelona tests; bottom left, sample prepared for SEM.

As for the specific curing, NC specimens were simply left in their moulds, while SC and EC specimens were demoulded at 4.5 h. At this time, concrete had already set and developed enough strength for the specimens to be placed in the curing equipment. SC specimens were stacked inside an environmental chamber with temperature and relative humidity kept constant at 25 °C and 98% respectively, until the onset of temperature cycle exactly at 5.5 h.

The stack was surrounded by 150 mm-thick expanded polystyrene to insulate all but the two large opposite faces, thus reproducing plane-like boundary conditions and minimising differences between the inner and the outer specimens of the stack. The environmental chamber was programmed for a linear temperature raise of 15 °C/h rate for 3 h, and then to keep constant 65 °C and 98% relative humidity for 7 h. At the end of the constant period, the system was allowed to cool down and reached 30 °C after approximately 24 h from mixing (see Fig. 3(a), dot-dot-dashed line).

As for the EC specimens, the same stacking and insulation setup was used (see Fig. 4). These specimens were individually wrapped immediately after demoulding in heat-shrinking plastic sheet to prevent moisture loss or electrical contact. The voltage was applied at the ends of each specimen separately so that the average direction of the electric current was approximately parallel to the length of the specimen.

The EC rig was housed in a controlled-climate room set at 22 °C (±1 °C) and 65% relative humidity. For a fair comparison between SC and EC, the average temperature measured inside the 4 specimens subjected to SC was taken as the target profile to reproduce using EC (see Fig. 3(a), circle-marked line). This was accomplished by adjusting the electric power, i.e. by variation of the voltage applied to each individual specimen.

A clamping jig applied to the stack prevented any loosening of the electrode contact during curing. Optimal contact was verified by checking that further tightening of the clamp had no effect on the measured resistance. The electrodes were connected to four independent variable autotransformers (Variac) fed by power line Alternating Current at 50 Hz. This configuration allowed manual and independent adjustment of the voltage supplied to each specimen and automatic logging of the electrical response, with readings taken for both voltage and current every 18 s. Voltage and current waveform readings at a sampling frequency of 5000 Hz were performed to gain information on the response of the electric load in terms of impedance.

The surface temperature of NC and EC specimens was measured using a thermographic camera (see Fig. 4). However, due to uncertainty about the emitting characteristics of the plastic wrapping the surface and the constant evolution of the water layer bled underneath, the thermal field could not be read in absolute terms through this method but provides indications on the relative distribution of temperatures.

3.4. Mechanical testing and magnetic induction testing

Each specimen was notched and tested in a 3-Point Bending (3 PB) setup, with crack-mouth opening displacement (CMOD) control according to [10]. More data on the same specimens were obtained by cutting of new specimens unaffected by the cracks observed in the flexural test. Following the procedure described by Galeote et al. [35], two cubes free of any insert were obtained by wet-sawing each tested specimen at the four points where the temperature probes had been embedded (see Fig. 3). Four of such cubes were used to assess the compressive strength [14] for each set and the remaining underwent the Barcelona test [15–18]. This set-up allowed having the same casting and curing conditions for the concrete undergoing flexural and compression tests, allowing a meaningful parallel assessment of these properties. The Barcelona test is considered better suited as a material control or acceptance test, rather than for the assessment of the constitutive properties of SFRC. However, in this study it was used to collect additional data from the same specimens tested in bending and to compare the effect of accelerated curing methods.

Fibre orientation and local content variation due to uneven distribution may significantly affect the mechanical performance of SFRC and have been studied extensively by researchers (see for instance Laranjera et al. [36]). In the context of EC, the bulk electrical conductivity is also crucially influenced by the fibre distribution. Therefore, a specific assessment was undertaken in this study to assess the possible variation of distribution. Among many proposed techniques, the magnetic method by Cavalaro and Torrents [11–13] was chosen. This method relates the fibre content and orientation to the change of induction measured when the specimen is inserted in a magnetic coil.

Notwithstanding the specific casting procedure consistently applied and described above and in order to prevent that mechanical and electrical properties could be related to a peculiar fibre content or orientation existing in the specimens, the magnetic data was analysed according to the following procedure. Firstly, the Shapiro-Wilk test was run to confirm the assumption of normality (threshold at $p = 0.05$) for both the contents and orientation numbers when grouping together all specimens with the same fibre dosage. Secondly, the ANOVA F-test was applied after grouping EC specimens on the one hand and NC and SC specimens on the other; the lowest p-values found were 0.992 for the content data and 0.192 for the orientation number, confirming that no statistically significant differences were present, and the specimens can therefore be considered homogeneous when the fibre system is concerned. Small material samples for the microstructural analysis were wet-sawn from the central part of the beam, at a distance of about 50 mm from the cracked section (see Fig. 2). To hinder further hydration that could reduce the differences in the microstructure, samples underwent a procedure close to the freeze-drying described by Zhang and Scherer [37]. First, the were placed in a refrig-
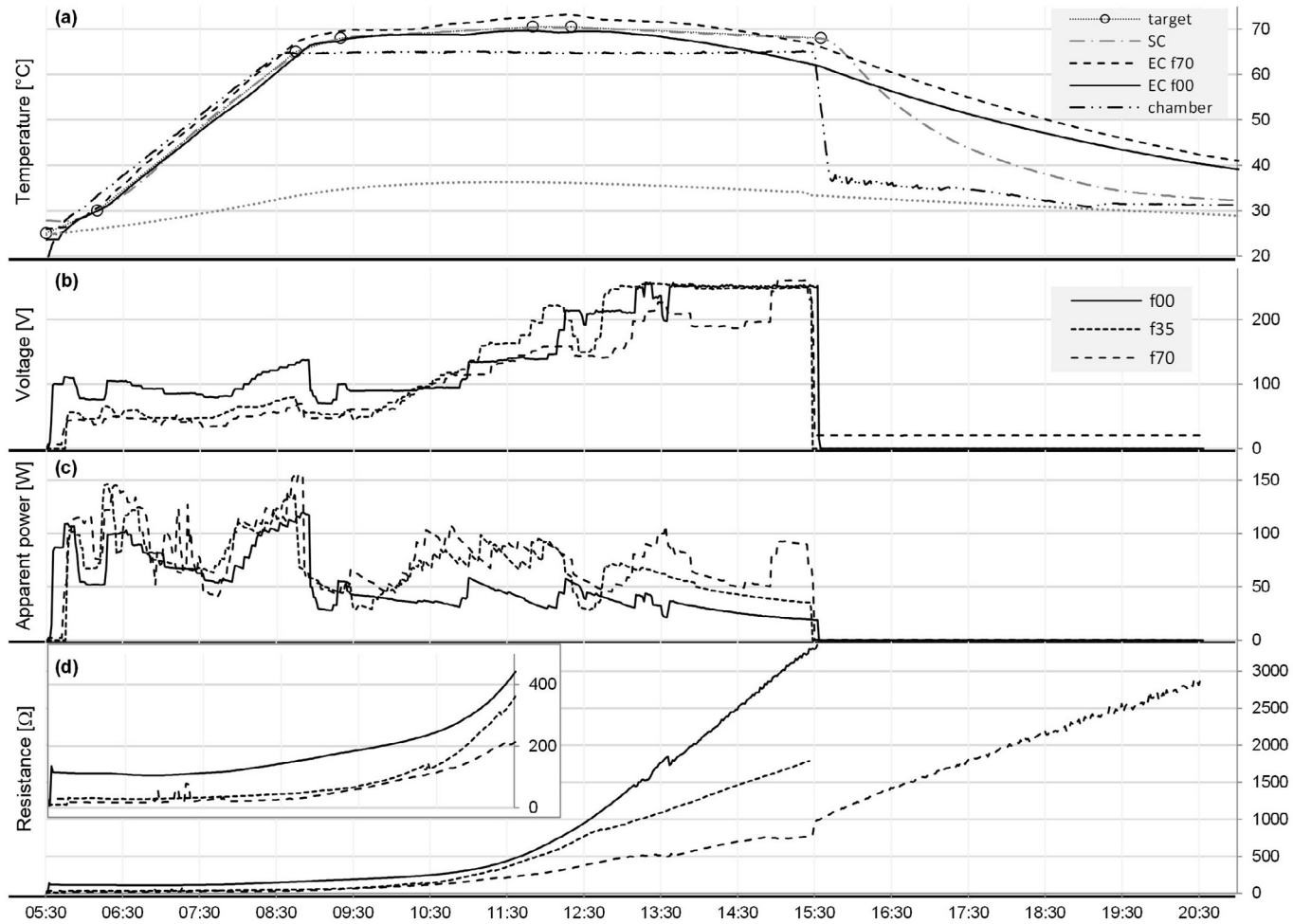
Fig. 3. Evolution of average temperatures over time after mixing for NC, SC and EC (a), evolution of voltage (b), apparent power (c) and resistance (d) over time for EC.

Fig. 4. EC specimens stacked in the electric rig.

erator at −38 °C for 24 h and, then, dried for 72 h to remove capillary water. Finally, the samples were placed in a container with magnesium perchlorate hydrates to maintain their low humidity until testing.

SEM (Scanning Electron Microscopy) was performed with a JEOL JSM 7100F microscope, at the voltage of 20 kV. Backscattered electron images and EDX (Energy Dispersive X-ray) analysis were obtained using this configuration. The SEM investigation was conducted on fragments that included a portion of a steel fibre (Fig. 3) partially encased by the matrix.

4. Results and discussion

4.1. Temperature evolution during curing process

Fig. 3(a) shows the evolution of the temperature inside the concrete over time during the curing. Each curve is the average of the four specimens considering the two innermost probes in each specimen. This temperature can be considered representative for the mid-span area that will experience crack formation. NC specimens (dotted line) show a maximum temperature of 37 °C after about 11.5 h due to the heat of hydration.

Observations made on SC specimens (dotted-dashed line) confirmed that the average internal temperature of the concrete is affected by its thermal inertia, as at the beginning it remains below the temperature of the chamber. The material temperature then rises above that of the chamber as the exothermal reaction of the cement hydration picks up, with a maximum average temperature inside the concrete of nearly 70 °C at 12 h after cement mixing (6.5 h after initiation of thermal treatment).

The continuous adjustment of the voltage applied to each specimen in EC kept the temperature within a range of ±3 °C of the average target value provided by the equivalent specimens subjected to SC. The only exception was found for the mix without fibre (f00), which showed a more pronounced drop after 13.5 h of accelerated curing. At this moment, the electric rig reached its maximum voltage of 250 V, being unable to generate additional power to cope with the high resistance of the specimen and to increase the temperature.

To provide a deeper insight into the EC, Fig. 3(b–d) shows the evolution over time of average voltage, apparent power and resistance, respectively for mixes f00, f35 and f70. It is worth noting that the voltage applied had to be increased over time to compensate for the rising resistance, and as a result the electric current decreased. This is in line with data from the literature [9,21,26,27,28] and may be the result of the reduction both in content, quality and continuity of the unbound liquid phase due to the evolution of the hydration process.

It can be concluded that the evolution of resistivity over time in all mixes follows a similar trend, remaining at low values at the beginning and presenting a rapid increase after 6 h of accelerated curing. A closer analysis (see magnified view within Fig. 3(d)) shows that the inclusion of fibres significantly reduces the bulk electrical resistivity of fresh concrete as the conductivity of steel is 7–8 orders of magnitude higher than that of fresh concrete. In this sense, the role of fibre orientation needs to be stressed, since a negligible change in resistivity would arise if fibres are oriented perpendicular to the electric current field, while such change can be of an order of magnitude when fibres are positioned parallel to the field.

Assuming no statistical difference of fibre distribution among specimens (the hypothesis was confirmed in the statistical analysis of the fibre content and orientation), the averaged resistance of f35 and f70 during the temperature rise phase was respectively 14% and 27% smaller than that found for f00; by the end of the constant temperature phase, these differences had doubled. Given the significant increase observed in the resistance during the curing period, it can be assumed that the electrical behaviour of the fibre matrix interface does not evolve significantly. In other words, the effect on the bulk conductivity of SFRC is determined by the content and orientation of the fibres, but its evolution resembles that of PC.

The apparent power reported in Fig. 3(c) is the product of voltage and current and therefore implies that the load is perfectly resistive, i.e. with unitary power factor. This has been reported in the literature to be the case for PC [23] and confirmed by impedance measurement carried out in this investigation. For SFRC however, the analysis of current and voltage waveforms sampled at 5 kHz indicated that the load is slightly capacitive, with current leading voltage phasor by approximately 5° for f35 and by 9° for f70 at the onset of EC. These shift angles decrease linearly and become close to zero after about 8 h. Consequently, the minimum values for the power factor are $\cos(\phi) = 0.996$ and $\cos(\phi) = 0.988$ respectively, which may be assumed unitary for simplicity of analysis (like in a perfectly resistive medium).

The specific energy calculated by integrating the apparent applied power until the completion of the temperature cycle was 41, 54 and 64 kWh/m^3 for f00, f35 and f70, respectively. These values are in line with those found in the literature [4,9,21,22]. In general, the energy required for EC depends on the temperature and length of the cycle, the amount of cement and binder in the mix and the effectiveness of any insulation deployed.

Interestingly, the higher energy required to cure SFRC is due to higher heat losses caused by overheating of the extremities. In fact, the thermal gradients developed along the length of the specimens were radically different in mixes with and without fibres. Fig. 5 shows typical thermal images taken 3.5 h after the beginning of the EC. The most striking difference when comparing the images of Fig. 5(a) and (b) is that, while relatively higher temperatures are found at the centre of the specimen without fibres (red zones), the opposite happens in the specimens with fibres, as relatively higher temperatures were measured at the ends.

These results suggest that the mix without fibre is more homogeneous in terms of conductivity and so is the generated power density. The extremities remain colder in this case because of the heat dissipated at the boundaries. In contrast, the unfavourable orientation of fibres due to the wall effect near the electrodes creates a zone with (relatively) lower conductivity at both ends of the specimen in comparison with the central part where fibres align more with the average direction of the electric field. Consequently, a higher power is generated, and the temperature rises more quickly at the ends due to the higher resistivity, as reported by Paillere [9].

Hot spots could be exacerbated by further increasing the matrix resistivity where maturity progresses faster due to higher temperature, leading to an even higher power density and run-away overheating. Although this phenomenon must be considered when designing an EC application, it affected only marginally the results of this investigation as the temperature of the central section was controlled throughout the curing process.

4.2. Mechanical strength

The black lines in Fig. 6(a) and (b) show the average flexural response of the f70 beams, while the corresponding envelope is delimited by grey lines; different dashings are used for the three different curing methods. It can be immediately observed that both SC and EC are effective in accelerating the evolution of flexural strength. At 1 day, SC and EC specimens have flexural strengths approximately 50% higher than that measured for NC specimens at the same age (see Fig. 6(a)). In fact, flexural strengths at 1 day in SC and EC specimens are very close to those reached in NC specimens at 28 days. Interestingly, the overall shape of the test curves remains similar regardless of the curing method or age, with a hardening branch until a CMOD (Crack Mouth Opening Displacement) of 0.7 mm and slowly diminishing afterwards.

As shown in Fig. 6(c) and (d), no further significant increase of the flexural residual strength was observed from 1 to 28 days, either in SC or EC specimens. Despite the potential influence of the change in the humidity condition of the specimen, these results suggest that the major part of the hydration took place during the first day after mixing. Results for f35 (Fig. 7) follow the same trend, with lower post-cracking values due to the smaller fibre content.

Fig. 8 shows the compressive strength (upper half) and the flexural strength (lower half) measured for all mixes and curing processes. For the latter quantity, the height of the bars shows the average value of the maximum flexural strength, f_x, and horizontal lines are drawn to indicate the average value of the cracking strength, f_{cr}. Notice that $f_x = f_{cr}$ in the case of f00, as fibres are not present to bridge the cracks; instead, the addition of fibres resulted in flexural hardening in f35 and f70 specimens, so that $f_x > f_{cr}$. Error bars indicate maxima and minima in each set, so to visually show the variation of the results. The statistical F-test was performed to evaluate if the differences observed in the comparison were statistically significant. The significance value (p-value) was considered 0.05. Consequently, statistically significant differences in the results should yield a p-value smaller than 0.05.

EC and SC specimens showed nearly identical cracking flexural strengths, with no systematic variation for all ages, fibre content and curing type (i.e., p-value >0.05 in all comparisons). This confirms that the strength of concrete matrix is not adversely affected by EC [9,21], even when fibres are present.

A different conclusion is derived from the analysis of the maximum flexural strength measured for mixes with fibres (after cracking has taken place). In this case, EC specimens consistently exhibited slightly inferior strength values than equivalent SC specimens. Such observation becomes more evident as the fibre content increases and at earlier ages, although differences are not statistically significant (p-value >0.05 in all comparisons). Similar trends are also observed for other parameters from the flexural tests that quantify the post-cracking performance. As an example,
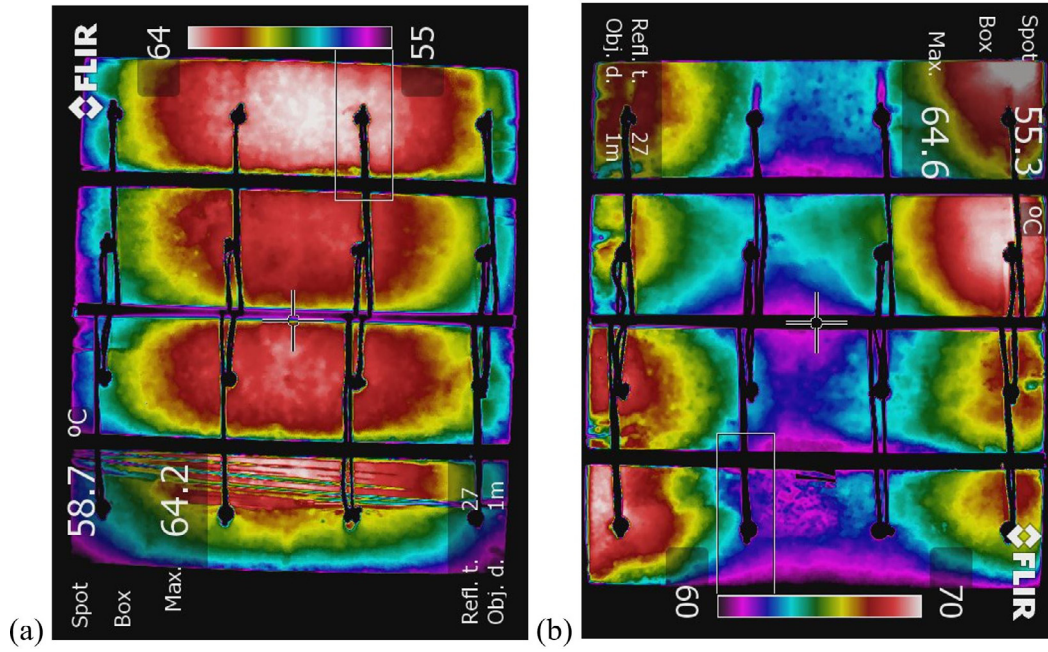
Fig. 5. Typical thermal images taken at 3.5 h for specimen without (a) and with fibres (b) subjected to EC.
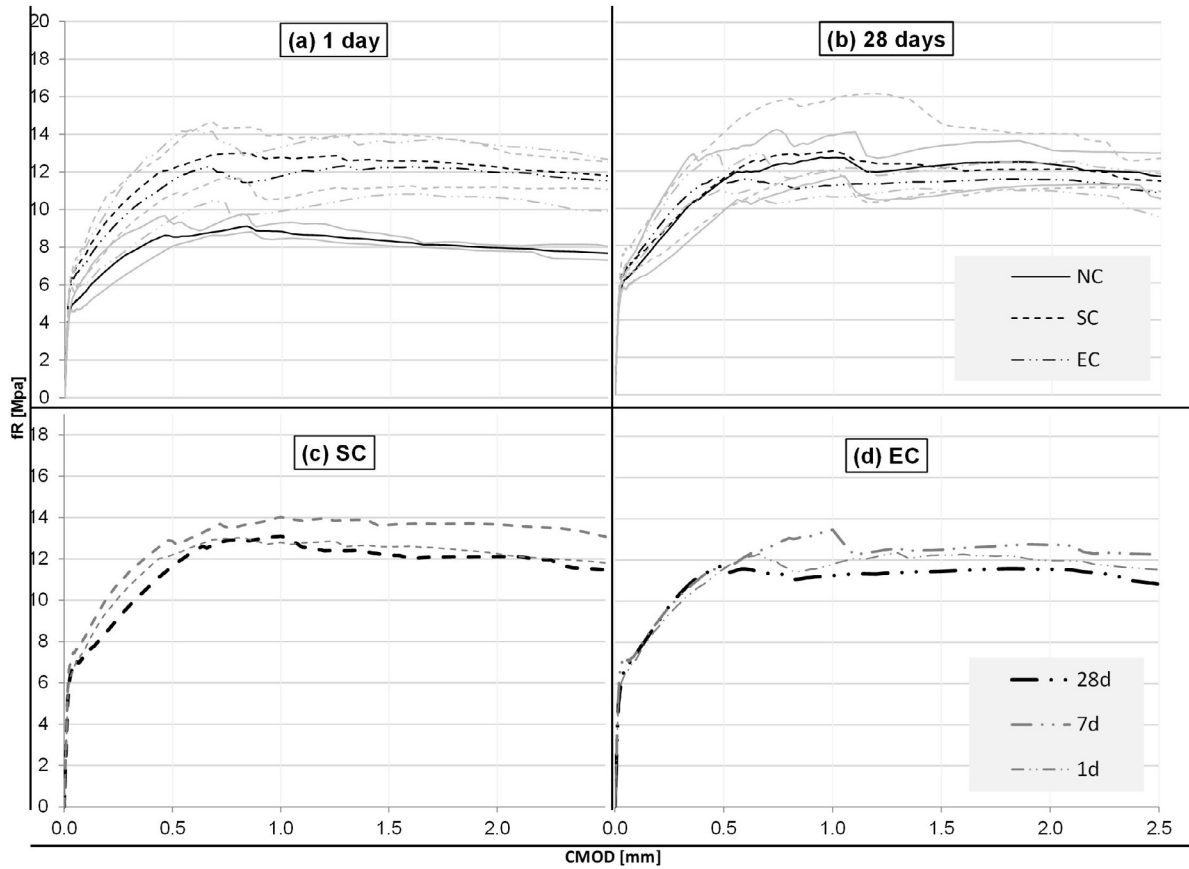
Fig. 6. Average and set envelope of Flexural strength-CMOD curves for mix f70: all curing methods at 1 day (a), all curing methods at 28 days and comparison at different ages for SC (c) and EC (d).
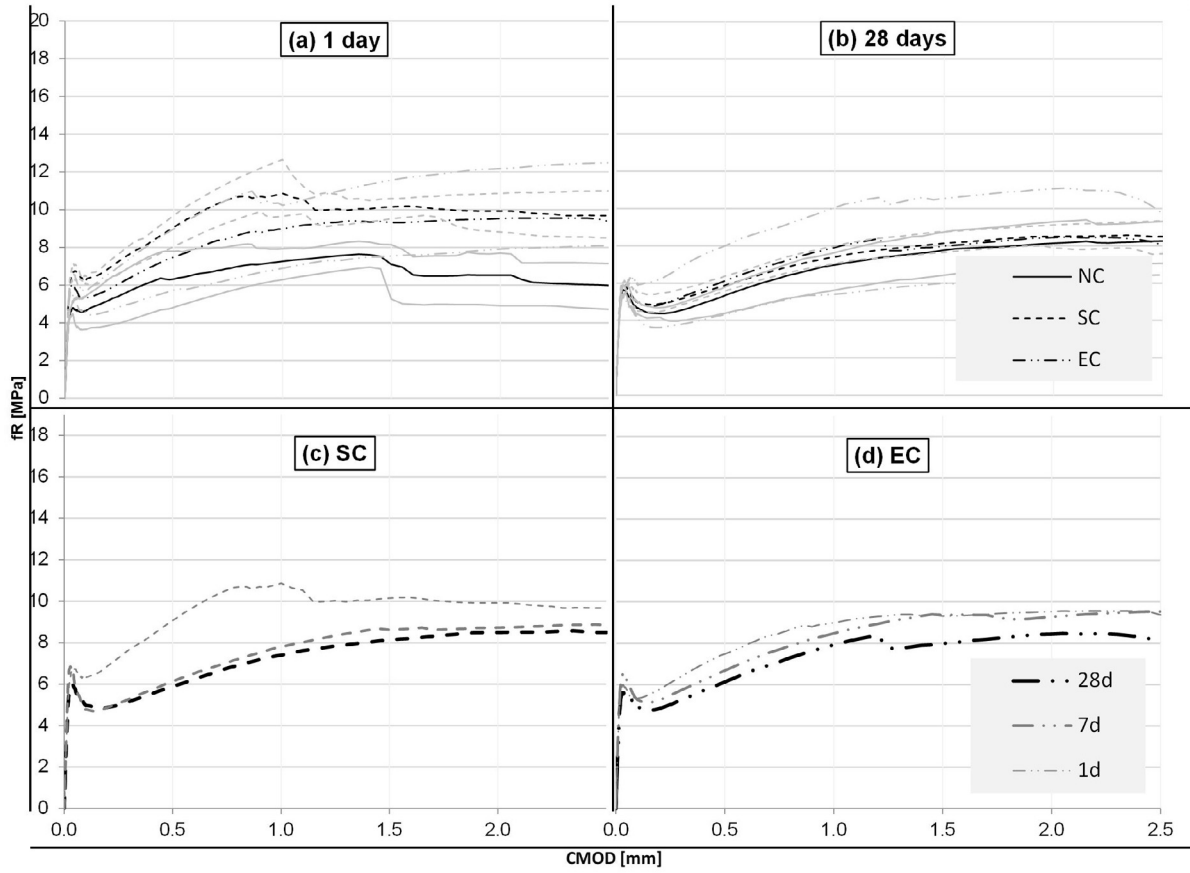
Fig. 7. Average and set envelope of Flexural strength-CMOD curves for mix f35: all curing methods at 1 day (a), all curing methods at 28 days and comparison at different ages for SC (c) and EC (d).
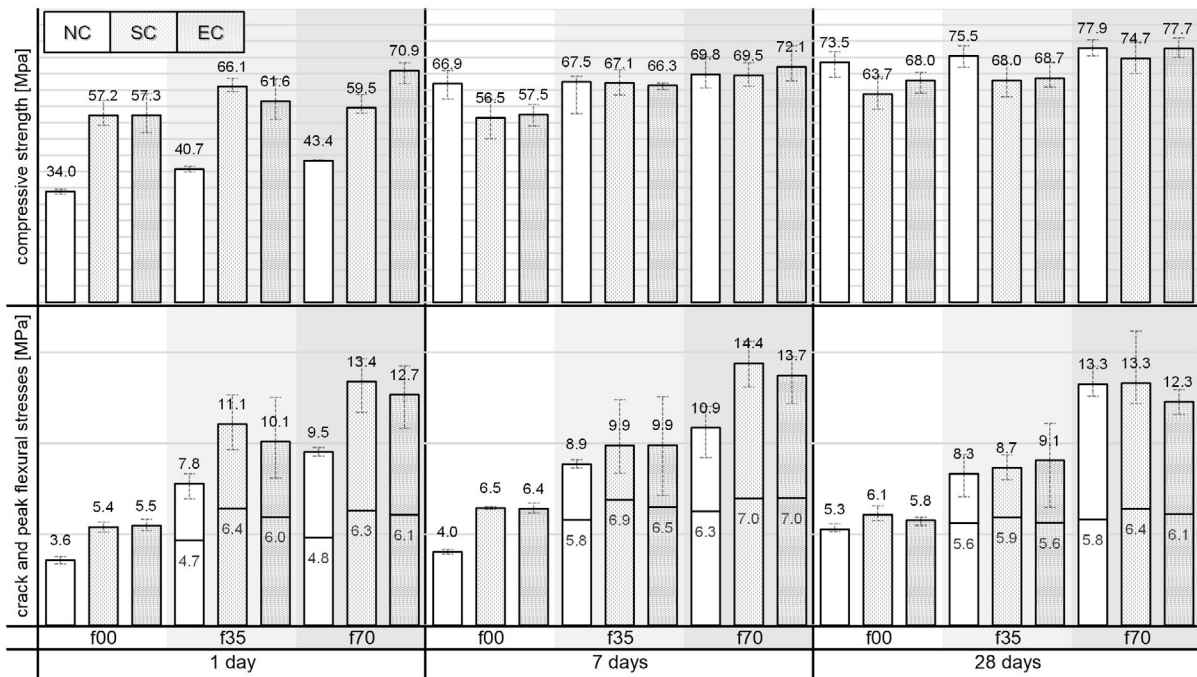
Fig. 8. Results of compressive strength testing obtained with sawn cubes and flexural cracking and peak strengths.

Fig. 8 shows the flexural residual strengths and the energy for the CMOD of 2.5 mm, and also in this case the values of EC specimens are slightly lower than those of equivalent SC specimens. Once more, these differences were not statistically significant (p-value >0.05).

Fig. 9 also reports the energy values from the Barcelona test. However, due to the high scatter of the results, it is not possible to confirm or reject any correlation with the trend observed from the bending tests. It must be noted that the cubes for splitting tests were sawn from portions of the beams whose temperature was not always within control during EC (see Fig. 5), which could have contributed to the scatter of these results.

The fact that a trend of lower values for EC is observed for the maximum flexural strength at the post-cracking stage, but not for the cracking strength, suggests that the EC might generate small modifications at the fibre-matrix interface. If this happened, then the cracking load would remain the same for both curing methods, as it depends mostly on the matrix, whereas the differences of maximum flexural strengths would be induced by the modification caused by EC in the fibre-matrix interface. Such

hypothesis will be further investigated in Section 4.3 through microstructural analysis of the interface.

Fig. 7 (upper half) also shows compressive strengths measured for all mixes and curing processes using the cube specimens cut from the beams. In general, mixes with fibres showed higher compressive strengths compared to the one without fibres, regardless of the age and curing process. This increase is consistent with results reported by Aydin [38], and it can be attributed to the additional confinement provided by the steel fibres to the matrix at high fibre contents.

At 28 days, SC and EC specimens had lower compressive strengths than reference NC ones, as typically observed when using heat accelerated curing [2]. Differences were statistically significant for f00 and f35. At 28 days, SC and EC specimens had average compressive strengths which are 14% and 8% lower than that found for equivalent NC specimens (p = 0.013 and p = 0.063) for the f00 mix and 10% and 9% lower than that found for equivalent NC specimens (p = 0.035 and p = 0.028) for the f35 mix.

No clear trend or statistically significant differences were found between the compressive strengths obtained with SC and EC,
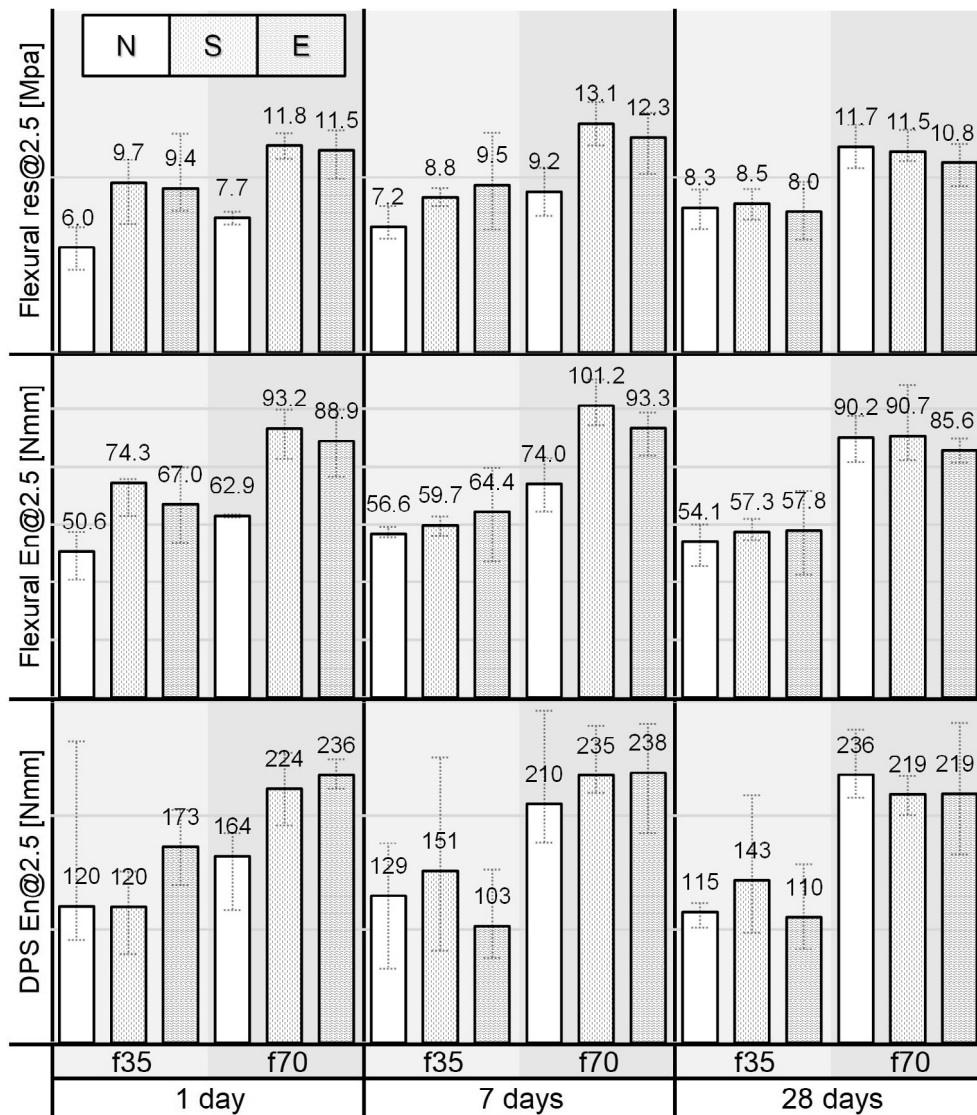
Fig. 9. Test results: of flexural residual strength for CMOD of 2.5 mm (top), flexural energy values for CMOD of 2.5 mm (middle) and Barcelona test energy at 2.5 mm penetration (bottom; notice that flexural testing was not carried out on f00).

regardless of the presence of the fibres. This confirms that the EC does not affect the performance of the matrix. It also reinforces the hypothesis that the slightly smaller post-cracking flexural performance of EC specimens could be related to changes at the fibre-matrix interface, which would only be perceived once cracks are formed and the fibres become active.

Interestingly, the compressive and the average flexural cracking strengths increase over time in all mixes and curing conditions, including SC and EC, while this trend is absent (if not reversed) in the evolution of the post-cracking residual strength of mixes subjected to SC and EC. Such result suggests that, although the additional hydration taking place from 1 to 28 days can improve the characteristics of the matrix responsible for the compressive and flexural cracking strengths, it does not seem to have the same impact in the fibre-matrix interface that governs the residual response. Since the main contribution during the pull-out of the fibres comes from the bending of the anchors, and the concrete's modulus of elasticity tends to develop much faster than the strength [39], a possible explanation of this disparity is that, provided that the fibre's tunnel is strong enough to resist crushing locally, the stiffness of the concrete matrix becomes a major parameter in establishing the post-cracking residual strength of the mix. Furthermore, an in-depth analysis of the variability of the results indicated no evident trend or significant differences in all comparisons made between SC and EC specimens.

4.3. Microstructural analysis

As the efficiency of SFRC is greatly dependent on the bond between fibres and matrix, the microstructural analysis was focused on the interfacial zone. Chan [40] suggested that bond failure can either occur at the fibre-paste contact surface (adhesive failure) or within the heterogenous transition zone (cohesive failure).

When applying EC, additional concerns emerge, as this zone also plays a crucial role in the electric conduction mechanism: metallic fibres have an electronic type of conductivity, i.e. electrons are the charged particles that move across the medium, in contrast to the ionic type taking place in the pore solution where ions are involved. Since fibres contribute to the bulk conductivity of the composite by bridging regions of pore solution with different electric potential, each fibre acts like an electrode in an electrolyte, and electrochemical phenomena may occur, even though stable electrolysis of water is only possible with direct current and not with alternating current [41]. This aspect thus requires adequate attention; nevertheless, to the best of the authors' knowledge, it has never been investigated in any published work.

Fig. 10 shows a comparison of surfaces of fibres pulled out from NC 9(a) and EC 9(b) samples. In both cases the fibres look relatively clean, with regular longitudinal grooves, likely to be due to the drawn-wire manufacturing process. No apparent sign of oxidation or corrosion in either NC or EC is observed. In general, more products of hydration appear adhered to the latter, as it can be seen in the magnified rectangles in Fig. 10(a) and (b). Although the difference is not such to suggest that a completely different failure mechanism has taken place, it could indicate small variations in the fibre-matrix interface zone.

Fig. 10 shows a comparison of the surface morphology of the cavity left by the pulled-out fibre in SC (11(a) and (c)) and EC (11(b) and (d)) specimens tested at an age of 1 day. The surface in contact with the fibre is more porous in the case of specimens subjected to EC in comparison with that subjected to SC. Such microstructural difference was, however, not sufficient to produce a statistically significant change in the post-cracking residual response observed in the mechanical tests. One possible explanation may be that the increase in porosity is not significant in the case of EC specimens. Another explanation could be that the resistance provided by the mechanical straightening of double-hooked fibres during the pull-out conceals the contribution of the surface friction induced by the variation in porosity.

Fig. 11 shows a back-to-back comparison of the surface morphology of the cavity left by a fibre in SC (11(a) and (c)) and EC (11(b) and (d)) after 1 day. The microstructure appears signifi-
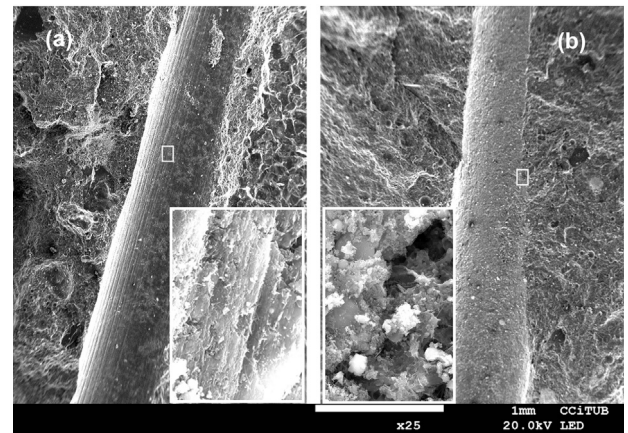
Fig. 11. SEM image of cavity left by fibre from 1d SC (a) and 1d EC (b); higher magnifications (4300×) reveal more porous morphology from EC.
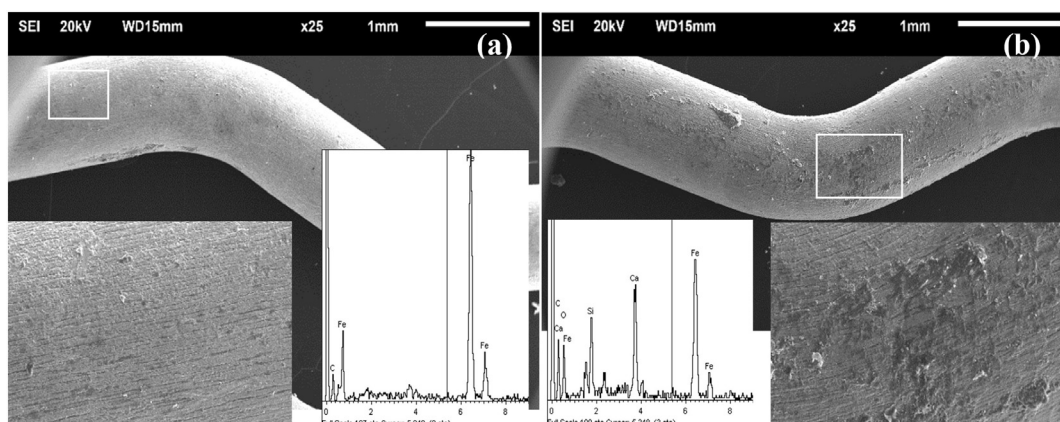
Fig. 10. SEM image and EDX spectra of a fibre pulled out from NC (a) and EC (b) specimens.
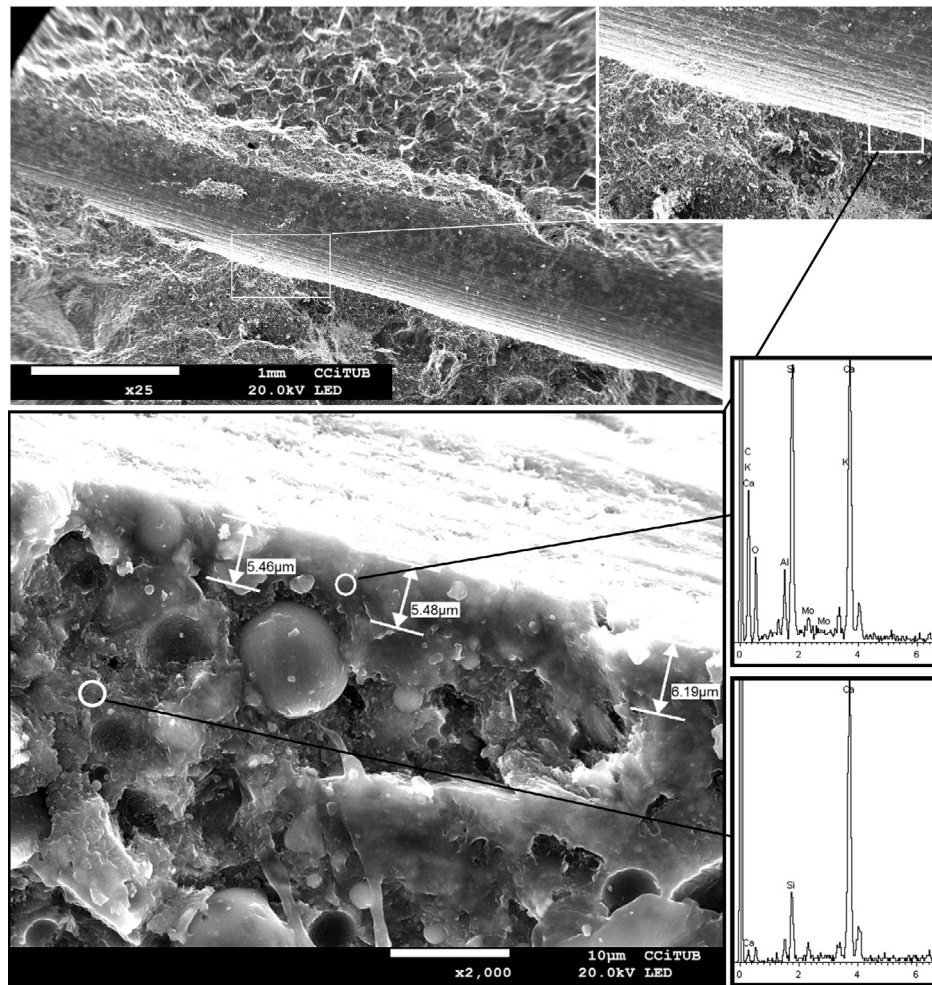
Fig. 12. Thickness and EDX spectra of the interfacial zone, SC.

cantly more porous after EC and the drawn grooves are not left imprinted as they are in SC.

Figs. 12 and 13 report a quantitative assessment of the transition zone after SC and EC, respectively. The formation of a denser cake-like layer being the result of silica fume precipitation is present in both cases, albeit its thickness is reduced by about 50% in the EC case. The formation of such a layer at the fibre interface has been reported in the literature [42]; however, without SF addition this layer is typically richer in calcium hydroxide crystals.

5. Conclusions

This study has built on the existing knowledge about EC (Electric Curing) and provided additional data and empirical evidence regarding its application to SFRC (Steel Fibre Reinforced Concrete), with an emphasis on its influence in the post-cracking performance. Results derived from the experimental programme confirm the feasibility of applying EC in elements made with SFRC.

The following conclusions can be drawn from this study:

a. The evolution of the conductivity of concrete over time should be considered for the design of the rig used for EC. The inclusion of fibres leads to a reduction of the resistivity of concrete, requiring the application of decreased voltage to achieve a certain temperature compared to a concrete without fibres. Despite this advantage, variations in the fibre distribution and orientation due to the wall effect can create zones with different conductivity within the volume of the element. This favours heat concentration and differences of temperature in the specimen. Fibre aspect ratio is likely to play a role in this aspect, but this study was limited only to one fibre typology.

b. The analysis of the mechanical properties of specimens produced with EC indicate that approximately the same mechanical properties can be obtained as SC for specimens with and without fibres, if the same temperature curve is applied. This suggests that the influence of EC in the evolution of properties of the matrix is similar to that of SC, being mainly governed by the temperature induced – not by electrochemical processes. This is consistent with previous studies available in the technical literature for PC, and it is now also confirmed for SFRC for the first time.

c. The 1-day strength of specimens subjected to accelerated curing (both EC and SC) was 50% higher than that observed in specimens subjected to NC (Fig. 7). At 28 days, EC and SC specimens showed poorer mechanical performance compared to equivalent NC specimens. No statistically significant differences between EC and SC were found in all mixes and different ages tested.

d. The compressive and the average flexural cracking strengths increase over time in all mixes and for different curing conditions (including SC and EC). A negligible evolution of the post-cracking residual performance is observed in mixtures subjected to SC and EC. Such result suggests that, although hydration is ongoing between 1 and 28 days which improves the characteristics of the matrix responsible for the com-
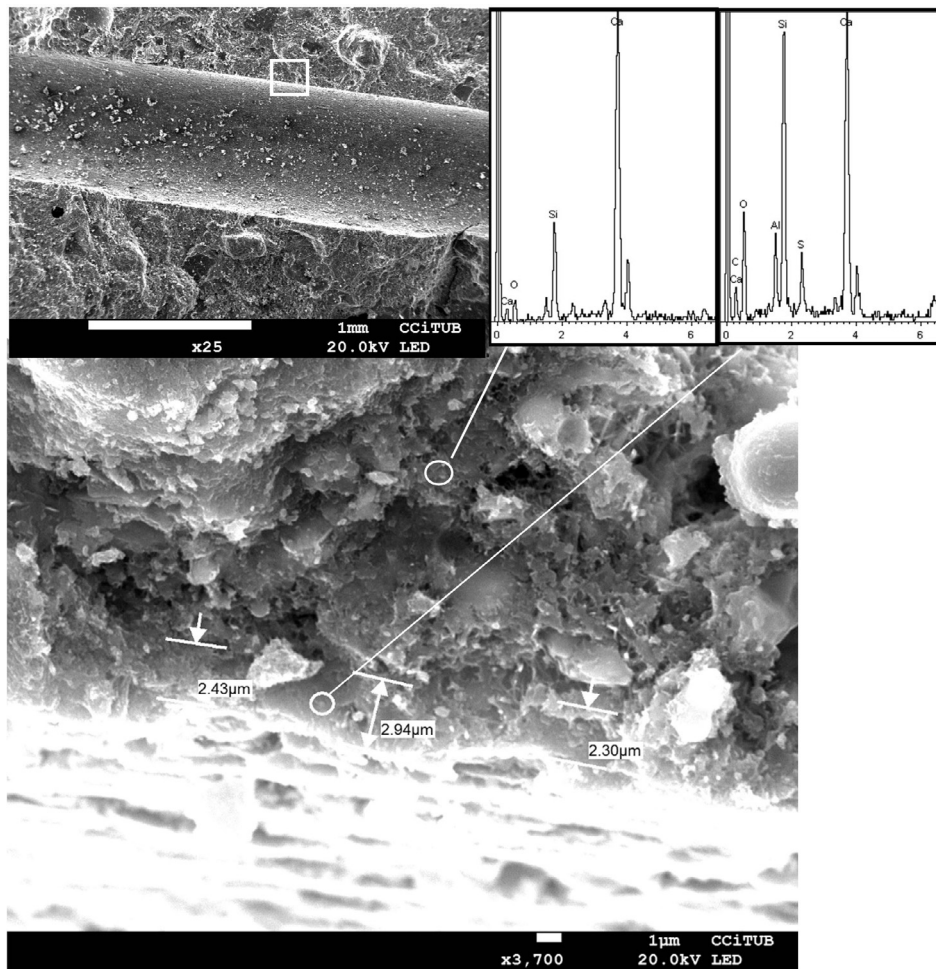
Fig. 13. Thickness and EDX spectra of the interfacial zone, EC.

pressive and flexural cracking strengths, it does not seem to have the same impact on the fibre-matrix interface that governs the residual response.

e. The post-cracking flexural response of EC specimens with fibres was repeatedly below that obtained for equivalent specimens subjected to SC. This trend was more evident at earlier ages and in specimens with the highest fibre content. Although differences are not statistically significant in any of the reported cases, such consistent observation suggests that EC could affect the microstructural characteristics or the composition of the matrix-fibre interface, producing a minor reduction of the flexural residual performance.

f. The microscopical analysis confirmed differences in the matrix-fibre contact area of samples subjected to EC and SC. A more porous interface was found in the case of EC, which may be responsible for the minor reduction in the post-cracking performance of the specimens. One possible explanation would be that transitional resistance appears at the interface due to a double electric layer formed by electrons in the metal and ions in the liquid phase of the matrix. This creates an obstacle for the passage of electric current and may originate expansion of air bubbles and drying caused by migration and evaporation of moisture near the surface, thus inducing higher porosity in the interface.

Further studies should be performed to confirm conclusion (f) and to analyse the presence of differences in terms of chemical composition at the interface. On the practical implementation of

the method, better electrode configuration should be devised to avoid overheating.

Acknowledgments

Conflict of interest

The authors declare that they have no conflict of interest.

References

[1] P.C. Taylor, Curing Concrete, CRC Press, Boca Raton, 2013.
[2] B. Vollenweider, Various methods of accelerated curing for precast concrete applications, and their impact on short and long term compressive strength, Concr. Technol. 241 (1) (2004) 1–22.

[3] J.D. McIntosh, Electrical curing of concrete, Mag. Concr. Res. 1 (1) (1949) 21–28.

[4] I.D. Kafry, Direct electric curing of concrete: basic design, Whittles (1993).

[5] W. Xuequan, D. Jianbgo, T. Mingshu, Microwave curing technique in concrete manufacture, Cem. Concr. Res. 17 (2) (1987) 205–210.

[6] A.M. Brandt, Fibre reinforced cement-based (FRC) composites after over 40 years of development in building and civil engineering, Compos. Struct. 86 (1–3) (2008) 3–9.

[7] A. Caratelli, A. Meda, Z. Rinaldi, P. Romualdi, Structural behaviour of precast tunnel segments in fiber reinforced concrete, Tunn. Undergr. Space Technol. 26 (2) (2011) 284–291.

[8] A. De la Fuente, P. Pujadas, A. Blanco, A. Aguado, Experiences in Barcelona with the use of fibres in segmental linings, Tunn. Undergr. Space Technol. 27 (1) (2012) 60–71.

[9] Paillere, A., Serrano, J. (1981). Utilisation de la conductivité des fibres métalliques dans le traitement thermique des bétons frais. Bull. Liason Labo. P. et Ch.113:59-61 (in French)

[10] EN 14651 (2005). Test method for metallic fibre concrete - measuring the flexural tensile strength (limit of proportionality (LOP), residual)

[11] S.H. Cavalaro, R. López-Carreño, J.M. Torrents, A. Aguado, P. Juan-García, Assessment of fibre content and 3D profile in cylindrical SFRC specimens, Mater. Struct. 49 (1–2) (2016) 577–595.

[12] S.H.P. Cavalaro, R. López, J.M. Torrents, A. Aguado, Improved assessment of fibre content and orientation with inductive method in SFRC, Mater. Struct. 48 (6) (2015) 1859–1873.

[13] J.M. Torrents, A. Blanco, P. Pujadas, A. Aguado, P. Juan-García, M.Á. Sánchez-Moragues, Inductive method for assessing the amount and orientation of steel fibers in concrete, Mater. Struct. 45 (10) (2012) 1577–1592.

[14] EN 12390-3, Testing Hardened Concrete. Part 3: Compressive Strength of Test Specimens, 2003.

[15] UNE 83515, Hormigones con fibras. Determinación de la resistencia a fisuración, tenacidad y resistencia residual a tracción (Fibre reinforced concrete. Determination of cracking strength, ductility and residual tensile strength), 2010.

[16] S.C. Malatesta, A.A. De Cea, C.M. Borrell, Generalization of the Barcelona test for the toughness control of FRC, Mater. Struct. 45 (7) (2012) 1053–1069.

[17] P. Pujadas, A. Blanco, S. Cavalaro, A. de la Fuente, A. Aguado, New analytical model to generalize the Barcelona test using axial displacement, J. Civ. Eng. Manage. 19 (2) (2013) 259–271.

[18] P. Pujadas, A. Blanco, S.H.P. Cavalaro, A. De La Fuente, A. Aguado, Multidirectional double punch test to assess the post-cracking behaviour and fibre orientation of FRC, Constr. Build. Mater. 58 (2014) 214–224.

[19] J. Reymann, Upcrete® and SCC – a new production method for precast elements to meet highest demands, Betonwerk und Fertigteil-Technik 75 (3) (2009) 30.

[20] D. Cecini, A. Palmeri, S. Austin, Beyond the floor cycle: integral casting of walls and floor slabs through double shutter formwork and SCC, 8th International RILEM Symposium on Self-Compacting Concrete, 2015, pp. 511–521.

[21] B.A. Krylov, Cold Weather Concreting, CRC Press, London, 1997.

[22] S. Bredenkamp, K. Kruger, G.L. Bredenkamp, Direct electric curing of concrete, Mag. Concr. Res. 45 (162) (1993) 71–74.

[23] J.G. Wilson, N.K. Gupta, Equipment for the investigation of the accelerated curing of concrete using direct electrical conduction, Measurement 35 (3) (2004) 243–250.

[24] I. Heritage, F.M. Khalaf, J.G. Wilson, Thermal acceleration of Portland cement concretes using direct electronic curing, Mater. J. 97 (1) (2000) 37–40.

[25] S.S. Wadhwa, L.K. Srivastava, D.K. Gautam, D. Chandra, Direct electric curing of in situ concrete, Build. Res. Inf. 15 (1–6) (1987) 97–101.

[26] H.W. Whittington, J. McCarter, M.C. Forde, The conduction of electricity through concrete, Mag. Concr. Res. 33 (114) (1981) 48–60.

[27] D.A. Whiting, M.A. Nagi, Electrical resistivity of concrete-a literature review, Portland Cem. Assoc. R&D Ser. (2003) 2457.

[28] Z. Li, X. Wei, W. Li, Preliminary interpretation of Portland cement hydration process using resistivity measurements, Mater. J. 100 (3) (2003) 253–257.

[29] P.L. Domone, Self-compacting concrete: an analysis of 11 years of case studies, Cem. Concr. Compos. 28 (2) (2006) 197–208.

[30] L. Ferrara, Y.D. Park, S.P. Shah, A method for mix-design of fiber-reinforced self-compacting concrete, Cem. Concr. Res. 37 (6) (2007) 957–971.

[31] H. Thooft, Reinforcing the future, Concrete 47 (1) (2014) 44–45.

[32] S.H.P. Cavalaro, A. Aguado, Intrinsic scatter of FRC: an alternative philosophy to estimate characteristic values, Mater. Struct. 48 (11) (2015) 3537–3555.

[33] T.K. Erdem, L. Turanli, T.Y. Erdogan, Setting time: an important criterion to determine the length of the delay period before steam curing of concrete, Cem. Concr. Res. 33 (5) (2003) 741–774.

[34] I. Soroka, C.H. Jaegermann, A. Bentur, Short-term steam-curing and concrete later-age strength, Matériaux et Construction 11 (2) (1978) 93–96.

[35] E. Galeote, A. Blanco, S.H. Cavalaro, A. de la Fuente, Correlation between the Barcelona test and the bending test in fibre reinforced concrete, Constr. Build. Mater. 152 (2017) 529–538.

[36] F. Laranjeira, A. Aguado, C. Molins, S. Grünewald, J. Walraven, S. Cavalaro, Framework to predict the orientation of fibers in FRC: a novel philosophy, Cem. Concr. Res. 42 (6) (2012) 752–768.

[37] J. Zhang, G.W. Scherer, Comparison of methods for arresting hydration of cement, Cem. Concr. Res. 41 (10) (2011) 1024–1036.

[38] S. Aydın, H. Yiğiter, B. Baradan, Effect of steam curing on class C high-volume fly ash concrete mixtures, Cem. Concr. Res. 35 (6) (2005) 1122–1127.

[39] P.K. Mehta, P.J. Monteiro, Concrete: Microstructure, Properties and Materials, McGraw-Hill, 2006. p.95 figure 4.6.

[40] Y.W. Chan, V.C. Li, Effects of transition zone densification on fiber/cement paste bond strength improvement, Adv. Cem.-Based Mater. 5 (1) (1997) 8–17.

[41] J.W. Shipley, The alternating current electrolysis of water, Can. J. Res. 1 (4) (1929) 305–358.

[42] A. Bentur, S. Diamond, S. Mindess, The microstructure of the steel fibre-cement interface, J. Mater. Sci. 20 (10) (1985) 3610–3620.